Geomechanics and Engineering, *Vol. 37, No. 4 (2024) 383-393*
https://doi.org/10.12989/gae.2024.37.4.383

Investigation on the responses of offshore monopile in marine soft clay under cyclic lateral load

Fen Li[1], Xinyue Zhu[1], Zhiyuan Zhu[1], Jichao Lei[1,2,3] and Dan Hu*[1]

[1]*School of Naval Architecture, Ocean and Energy Power Engineering, Wuhan University of Technology, 1178 Heping Avenue, Wuchang District, Wuhan City, Hubei Province, China*
[2]*Key Laboratory of High Performance Ship Technology of Ministry of Education, Wuhan University of Technology, China*
[3]*State Key Laboratory of Hydraulic Engineering Simulation, Tianjin University, China*

(*Received September 4, 2023, Revised April 29, 2024, Accepted May 2, 2024*)

Abstract. Monopile foundations of offshore wind turbines embedded in soft clay are subjected to the long-term cyclic lateral loads induced by winds, currents, and waves, the vibration of monopile leads to the accumulation of pore pressure and cyclic strains in the soil in its vicinity, which poses a threat to the safety operation of monopile. The researchers mainly focused on the hysteretic stress-strain relationship of soft clay and kinds of stiffness degradation models have been adopted, which may consume considerable computing resources and is not applicable for the long-term bearing performance analysis of monopile. In this study, a modified cyclic stiffness degradation model considering the effect of plastic strain and pore pressure change has been proposed and validated by comparing with the triaxial test results. Subsequently, the effects of cyclic load ratio, pile aspect ratio, number of load cycles, and length to embedded depth ratio on the accumulated rotation angle and pore pressure are presented. The results indicate the number of load cycles can significantly affect the accumulated rotation angle of monopile, whereas the accumulated pore pressure distribution along the pile merely changes with pile diameter, embedded length, and the number of load cycles, the stiffness of monopile can be significantly weakened by decreasing the embedded depth ratio *L/H* of monopile. The stiffness degradation of soil is more significant in the passive earth pressure zone, in which soil liquefaction is likely to occur. Furthermore, the suitability of the "accumulated rotation angle" and "accumulated pore pressure" design criteria for determining the required cyclic load ratio are discussed.

Keywords: cyclic lateral load; monopile; plastic strain; pore pressure; soft clay; stiffness degradation model

1. Introduction

Globally, more than 75% of the existing bottom-fixed offshore wind turbine are founded on the large-diameter monopile for its excellent bearing capacity, ease of installation, and low cost. In the complex marine environment, the monopiles are subjected to cyclic lateral loads induced by winds (Yu *et al*. 2023, Gao *et al*. 2022), currents, and waves (Shi *et al.* 2022, Guth *et al*. 2023). Under moderate-to-high amplitudes of cyclic loading, the vibration of monopile leads to the accumulation of cyclic strains in the soil in its vicinity (Barari *et al.* 2021). The reduction in soil modulus and undrained shear strength degradation may occur due to the cyclic lateral loads (Thiers and Seed 1968, Gerolymos and Gazetas 2005).

In the previous studies, various soil stiffness degradation models have been developed to account for the changes in volumetric strain and pore pressure, such as the degradation index model (Idriss *et al.* 1978) and pore pressure model (Wang *et al.* 2018), and thus adopted to describe the accumulated deformation of monopile foundations under cyclic lateral load. Achmus *et al.* (2009) simulated the behavior of monopile under cyclic lateral loads numerically, using the cyclic stiffness degradation index and the stiffness degradation model of soil proposed by Idriss *et al*. (1978) and Huurman (1996), the design charts of monopile were developed for both static and cyclic load. Kuo *et al.* (2012) adopted the stiffness degradation model to investigate the accumulated deformation of monopile with various diameters, the different design criteria regarding the required minimum pile length were proposed. With the same model, Depina *et al.* (2015) analyzed the effect of the embedded length and the number of load cycles on the ultimate bearing capacity of monopile and further proposed that the accumulated deformation decreased significantly with the increase of embedded length. Hu *et al.* (2014) established the secant stiffness degradation model considering the soil stress state and investigated the accumulated deformation of large-diameter monopile foundation subjected to the horizontal cyclic loads. Abhinav *et al.* (2019) investigated the influence of stiffness degradation on the response of monopile-supported OWT embedded in clay under combined aerodynamic and hydrodynamic loads. Cui *et al*. (2023) compared the backbone curve and hysteretic curve of saturated soft clay under different confining pressure and different vibration frequencies through dynamic triaxial tests, and proposed the fitting model of the maximum dynamic shear modulus using a multiple linear regression method, the variation law of the fitting shear modulus ratio with shear strain was proposed. Wang *et al*. (2023) proposed a model for marine

*Corresponding author, Lecturer
E-mail: hudan1989.happy@163.com

ISSN: 2005-307X (Print), 2092-6219 (Online)

soft clay based on the dynamic triaxial tests, and analyzed the deformation responses of single-cylinder and four-cylinder suction pile foundations in soft clay subjected to horizontal cyclic loads. Feizi *et al.* (2023) developed the soil model with realistic hysteretic damping and non-linear springs, and adopted the soil model for earthquake analysis in time history.

In terms of pore pressure model, Yasuhara *et al.* (1982) conducted the cyclic triaxial tests and proposed that the accumulated pore pressure was highly related to the consolidation of soil, especially for high-frequency cyclic load. Matasović *et al.* (1995) proposed the predicted formula to reflect the accumulation of pore pressure with cyclic stiffness degradation index. According to the cyclic dynamic triaxial test results of saturated soft clay, Zhao *et al.* (2012) demonstrated that there is an exponential relationship between the accumulated pore pressure and the number of load cycles. Based on the dynamic triaxial test results, Liu *et al.* (2020) proposed the pore pressure accumulation model including the effect of cycle number. Cuéllar *et al.* (2013) analyzed the accumulation of residual pore water pressure in saturated soil around monopile under cyclic lateral loads and further concluded that the accumulation of residual pore pressure would significantly change the behavior of monopiles under external loads. Cui *et al.* (2019) investigated the effect of soil shear stiffness degradation on the accumulation of pore pressure through numerical method and demonstrated that the shear stiffness degradation accelerated the increase of pore pressure. Based on the cyclic triaxial test results, the stiffness degradation model of soft clay considering the pore pressure accumulation was proposed by Charlton *et al.* (2021), and further adopted to analyze the accumulated lateral deformation of large-diameter monopile foundations for offshore wind turbines under long-term cyclic loads.

The previous research work is mainly focused on the hysteretic stress-strain relationship of soft clay and kinds of stiffness degradation models have been implemented, which may consume considerable computing resources and is not applicable for the long-term bearing performance analysis of monopile. Thus, a simpler and more practical soil stiffness degradation model of clay is required.

In this study, an improved stiffness degradation model that considers the accumulated pore pressure and accumulated plastic strain is proposed. By working with the numerical concept, the proposed model has been implemented into ABAQUS and verified by comparing the predicted results with the undrained cyclic triaxial test results. A series of parametric studies are conducted to investigate the effects of cyclic load amplitude, number of load cycles, diameter, and embedded length on the cyclic behavior of monopile. Finally, the variation of the accumulated rotation angle and pore pressure under cyclic lateral load are discussed by introducing the safety factor, and some useful design guidelines are suggested.

2. Model implementation and verification

2.1 Stiffness degradation model

As observed from the undrained cyclic triaxial test

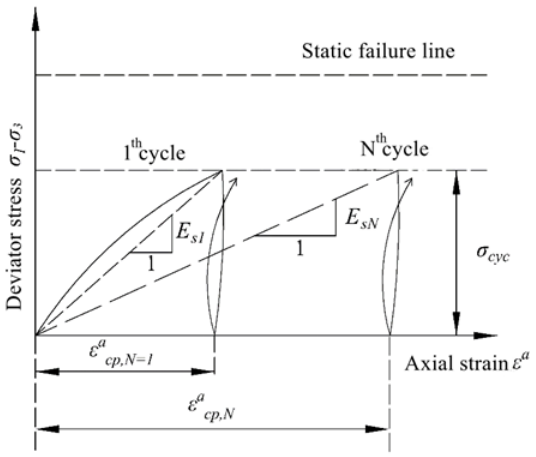

Fig. 1 Degradation of secant modulus under cyclic loading

results in Fig. 1, the plastic axial strain accumulates with the number of load cycles, the stiffness degradation model is proposed to account for the cyclic load effects. By assuming the elastic strain is negligible, the degradation rate of the secant stiffness is represented by the plastic axial strain $\varepsilon^a_{cp,N=1}$ and pore pressure $u_{N=1}$ after 1st cycle, plastic axial strain $\varepsilon^a_{cp,N}$ and pore pressure u_N after Nth cycle according to the following equations

$$\delta = \frac{E_{sN}}{E_{s1}} \cong \frac{\sigma'_{1,N}/\varepsilon_{cp,N}}{\sigma'_{1,N=1}/\varepsilon_{cp,N=1}} = \frac{\sigma - u_N}{\sigma - u_{N=1}} \frac{\varepsilon_{cp,N=1}}{\varepsilon_{cp,N}} \tag{1}$$

in which δ is the cyclic stiffness degradation index, E_{s1} and E_{sN} are the secant elastic modulus of soil after 1st cycle and Nth cycle, respectively, $\sigma'_{1,N=1}$ and $\sigma'_{1,N}$ are the major principal effective stress after 1st and Nth cycle, σ is the total axial stress.

The accumulation of plastic axial strain for each cycle $\varepsilon_{cp,N}$ was usually estimated using the semi-empirical approaches proposed by Huurman (1996), Gotschol (2009), and Werkmeister (2003). In this study, Huurman's formula (1996) is adopted, and the stiffness degradation can be described using two material parameters b_1 and b_2 as follows

$$\frac{\varepsilon_{cp,N=1}}{\varepsilon_{cp,N}} = N^{-b_1\left(X_{cyc}\right)^{b_2}} \tag{2}$$

in which N is the number of load cycles and X_{cyc} is the cyclic stress ratio defined by Huurman (1996) for cohesionless material as

$$X_{cyc} = \frac{\sigma_{1,cyc}}{\sigma_{1d,sf}} \tag{3}$$

where σ_(1,cyc) is the major principal stress at the cyclic stress state, σ_(1d,sf) is the major principal stress at the dynamic failure state. The cyclic stress ratio Xcyc is dependent on the confining pressure and cyclic stress level, Eqs. (2) and (3) are appropriate for the cyclic stress level is less than the critical value. Thus, the characteristic cyclic stress ratio is defined as

$$X_{cyc} = \frac{\sigma_{1,cyc} - \sigma_{1,ini}}{\sigma_{1d,sf}} \tag{4}$$

here $\sigma_{1,ini}$ is the major principal stress at the initial stress state. Zhao *et al.* (2012) suggested the major principal stress at the dynamic failure state could be defined as

$$\sigma_{1d,sf} = 0.6\sigma_{1,sf} \tag{5}$$

in which $\sigma_{1,sf}$ was the major principal stress at the static failure state, Eq. (5) was derived from the cyclic triaxial tests without the effect of static deviator stress, which has a significant effect on the accumulation of plastic strain and pore pressure.

Subsequently, Zhao *et al.* (2012) put forward an equivalent cyclic dynamic stress level that included the static deviator stress and cyclic dynamic deviator stress, which included the coupling effect of pore pressure and plastic strain. The coupled stress ratio X_c is thus defined as

$$X_c = X_{cyc} + K \cdot X_s \tag{6}$$

where X_{cyc} is the cyclic stress ratio, K is the equivalent coefficient and usually taken as 0.4 according to the triaxial test results and X_s is defined as equivalent cyclic stress ratio.

According to Eqs. (5) and (6), X_s can be rewritten as

$$X_s = \frac{\sigma_{1,s} - \sigma_{1,ini}}{\sigma_{1,sf}} \tag{7}$$

in which $\sigma_{1,s}$ is the major principal stress at the static deviator stress state.

According to the triaxial test results, Zhao *et al.* (2012) proposed that the pore pressure developed with the same trend as the plastic strain, the development of pore pressure could be represented by two material parameters a_1 and a_2 as

$$\frac{u_{N=1}}{u_N} = N^{-a_1\left(X_{cyc}\right)^{a_2}} \tag{8}$$

By substituting Eqs. (2)-(8) into Eq. (1), there is

$$\delta = \frac{E_{sN}}{E_{s1}} \cong \frac{1}{1-u'} N^{-b_1\left(X_{cyc}\right)^{b_2}} - \frac{u'}{1-u'} N^{-\alpha \cdot b_1\left(X_{cyc}\right)^{b_2}} \tag{9}$$

where $u' = \frac{u_{N=1}}{\sigma}$, α is the equivalent coefficient that can be obtained by fitting the triaxial test results.

Eqs. (6)-(9) are proposed for the triaxial tests under isotropic initial stress conditions and constant confining pressure σ_3 under the cyclic stress state. However, the initial stress conditions are anisotropic in the pile-soil interaction system, the minor principal stress as well as the direction of the principal stress axes generally changes with the application of the lateral load, as illustrated in Fig. 2.

In this study, based on the characteristic cyclic stress ratio proposed by Achmus *et al.* (2009), the characteristic coupled cyclic stress ratio X_{cc} is proposed and defined as

$$\begin{aligned} X_{cc} &= X_{c,cyc} + K \cdot X_{c,s} \\ X_{c,cyc} &= \frac{X_{cyc} - X^{(0)}}{1 - X^{(0)}}, \quad X_{c,s} = \frac{X_s - X^{(0)}}{1 - X^{(0)}} \end{aligned} \tag{10}$$

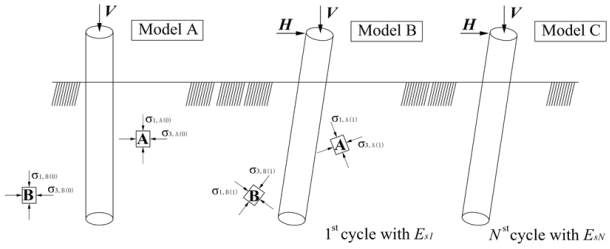

Fig. 2 Schematic sketch of the stiffness degradation in the pile-soil system

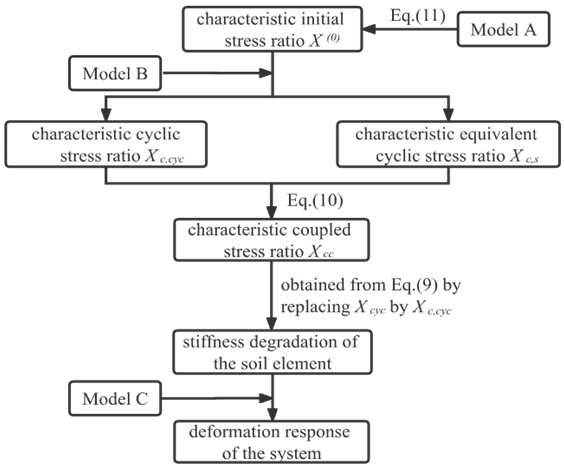

Fig. 3 Implementation process for the stiffness degradation model

in which $X_{c,cyc}$ represents the characteristic cyclic stress ratio as the cyclic lateral load is applied, $X_{c,s}$ gives the characteristic equivalent cyclic stress ratio as the static lateral load is applied, and $X^{(0)}$ is the characteristic initial stress ratio at unloading state, which can be defined as

$$X^{(0)} = \frac{\sigma_{1,ini} - \sigma_p^{(0)}}{\sigma_{1,sf}^{(0)}} \tag{11}$$

where $\sigma_p^{(0)}$ and $\sigma_{1,sf}^{(0)}$ are mean and major principal stress at static failure state, respectively.

At the initial or unloading phase (model A in Fig. 2), only the vertical load V is applied, the lateral load H is applied subsequently in the loading phase (model B in Fig. 2), in the last step of simulation (model C in Fig. 2), the deformation response of the system is analyzed using the stiffness degradation model obtained from models A and B with respect to Eqs. (9) and (10)

2.2 Implementation and verification

To implement the stiffness degradation model into the finite element program ABAQUS, the cyclic stiffness degradation index δ is defined as the field variable changes with the cycle number by using the USDFLD subroutine. By assuming the Poisson's ratio is constant, the implementation process for the stiffness degradation model is illustrated in Fig. 3. Specifically, the first step is to

Table 1 The material parameters of the saturated soft cla

E_s(MPa)	ρ_s(g/cm^3)	φ_{cu}(°)	c_{cu}(kPa)	v_s	e_0	k_s(m/s)
6.0	1.93	20	6.5	0.37	1.07	1×10^{-8}

* E_s: Compression modulus; ρ_s: Density; φ_{cu} : Friction angle; c_{cu}: Cohesion; v_s: Poisson's ratio; e_0: Void ratio; k_s: Permeability coefficient

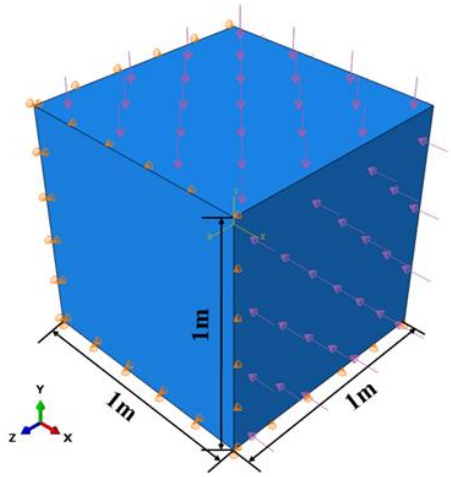

Fig. 4 The numerical model of soil element

calculate the characteristic initial stress ratio $X^{(0)}$, thus the characteristic cyclic stress ratio $X_{c,cyc}$ and the characteristic equivalent cyclic stress ratio $X_{c,s}$ can be determined. Subsequently, the characteristic coupled stress ratio X_{cc} can be derived according to Eq. (10). The stiffness degradation of the soil element is obtained from Eq. (9) by replacing X_{cyc} with $X_{c,cyc}$. In the last step of the simulation (model C), the deformation response of the system is analyzed using the stiffness degradation obtained from models A and B with respect to Eqs. (9) and (10)

The stiffness degradation model is further verified by comparing the numerical results with the cyclic triaxial test results conducted by Huang *et al.* (2006). For the simulation of the soil behavior, an elasto-plastic material with Mohr–Coulomb failure criterion is used. The material parameters of the saturated soft clay are given in Table 1.

The soil is meshed with 8-node brick element as shown in Fig 4. In the stress-controlled undrained (CU) cyclic triaxial test, the vertical displacement is fixed at the bottom boundary, the uniform confining pressure p_c are applied along the lateral boundaries. The static deviator stress η_s with different amplitudes are applied on the undrained top surface, the one-way cyclic deviator stress η_d with different amplitudes are applied subsequently.

The numerical results are compared with the experimental results under different confining pressure p_c=100 kPa and p_c=200 kPa, as shown in Figs. 5 and 6, respectively. It is observed that as the number of load cycles N is more than 3000, the calculated accumulated axial strain and pore pressure are generally consistent with the experimental results. With the increase of cycle number, the discrepancies between them are getting smaller, which indicated that the proposed stiffness degradation model can generally capture the permanent deformation responses of soil element. By comparing the cyclic test results with

Table 2 The ranges for model parameters

Pile geometry	Loading
Embedded length H 30-50 m	One-way static lateral load M_s 0.26-1.43MN
Diameter D 6.5-8.5 m	One-way cyclic lateral load M_d 1.3-13 MN
	Number of load cycles N 10^4-10^8

numerical results, the typical regression parameters b_1, b_2, α, and u' are determined, i.e., b_1=0.078, b_2=0.115, α=4.141, and u'=0.514, the fitted parameters are adopted in the following studies.

3. Parametric study

By virtue of the proposed stiffness degradation model, the parametric studies are carried out to quantify the effects of cyclic load amplitude, cycle number, pile diameter, and embedded length on the behavior of monopile embedded in soft clay. The ranges for model parameters were listed in Table 2.

3.1 Model parameters

In this study, the long-term wind and wave loads exerted on the monopile are considered as one-way cyclic lateral load, and current load as one-way static lateral load. For cylindrical structures with D/λ (diameter to wave length ratio) less than 0.2, the wave load is calculated by Morison equation and written as

$$F_H = \int_0^h \frac{1}{2} C_D \rho D u_x |u_x| dz + \int_0^h C_M \rho \frac{\pi D^2}{4} \frac{\partial u_x}{\partial t} dz \quad (12)$$

in which h is water depth, ρ is water density, u_x is the horizontal wave speed, and C_D and C_M are drag force and inertia force coefficient, respectively.

The wind load can be calculated by the design standard of China (GB 50009-2012) and expressed as

$$F_f = \omega \beta_s \beta_z p_0 A, \ \ p_0 = \frac{V_f^2}{1600} \quad (13)$$

where ω, β_s, β_z are empirical coefficients, p_0 is the basic wind pressure, A is the loaded area, and V_f is the wind speed.

The current load can be simplified as dynamic pressure

$$F_w = \frac{1}{2} C_w \rho A V_w^2 \quad (14)$$

where C_w is the drag force coefficient, and V_w is the current speed.

Therefore, the one-way static lateral load M_s and cyclic load M_d are expressed as

$$M_s = F_w, \ M_d = F_H + F_f \quad (15)$$

In establishing the soil-pile interaction system, the soil is considered as elastic-perfectly plastic material, the pipe pile was equivalent to a solid pile. The material parameters

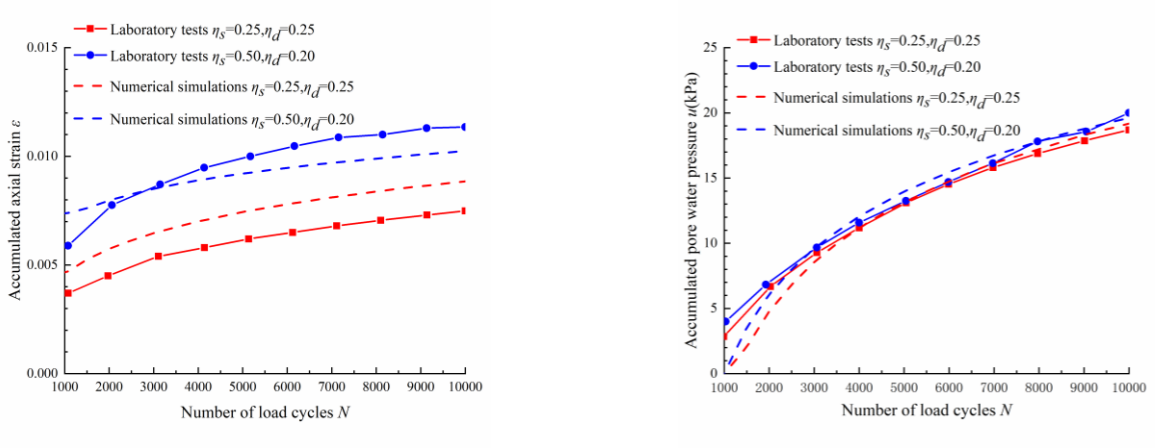

Fig. 5 Axial strain and pore pressure accumulation of saturated soft clay (p_c=100 kPa)

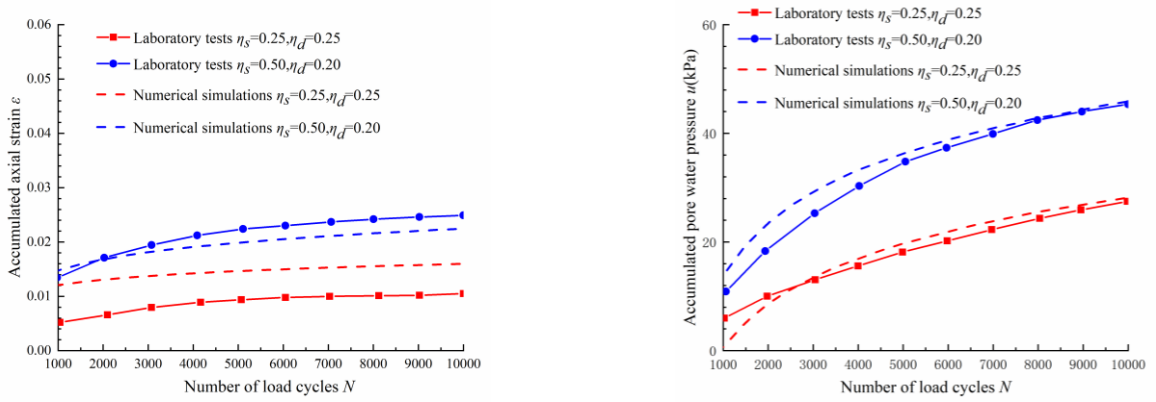

Fig. 6 Axial strain and pore pressure accumulation of saturated soft clay(p_c=200 kPa)

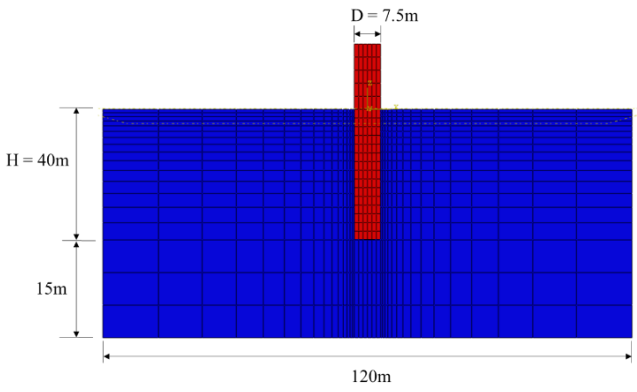

Fig. 7 The soil-pile interaction model

Table 3 The material parameters of solid pile

D (m)	L(m)	H(m)	ρ_{pE}(g/cm^3)	E_{pE}(GPa)	v_p	D (m)
7.5	60	40	0.372	19.45	0.3	**7.5**

* D: Diameter; L: Length; H: Embedded length; ρ_{pE}: Equivalent density; E_{pE}: Equivalent elastic modulus; v_p: Poisson's ratio

of solid pile are illustrated in Table 3. Due to the symmetry of the load and structure, only half of the soil-monopile interaction model is established as illustrated in Fig. 7. To avoid boundary effect, the diameter and height of the soil domain are taken as 16D and L. The plane of symmetry is constrained in the normal direction, the bottom boundary is fixed in the vertical direction and the top is set as undrained, the lateral boundaries are laterally constrained. The 8-node linear brick element with reduced integration (C3D8R) is adopted for the monopile, and 8-node brick with pore pressure elements (C3D8RP) is used for meshing the soil domain, there are a total of 440 pile elements and 2766 soil elements.

The soil-pile interface is defined by the mechanical contact properties, including the normal and tangential behavior of the contact surface. For the normal behavior, no separation is permitted, whereas the tangential behavior is simulated by Coulomb friction model, which is defined by $\tau_{crit} = \mu P$, where τ_{crit} is the ultimate shear stress, P is the ultimate stress, μ is the friction coefficient, $\mu = 0.24$ is adopted in this study.

3.2 Influence of cyclic load amplitude

To quantify the effect of cyclic load amplitude, the non-dimensional static load ratio ζ_s and cyclic load ratio ζ_d are introduced

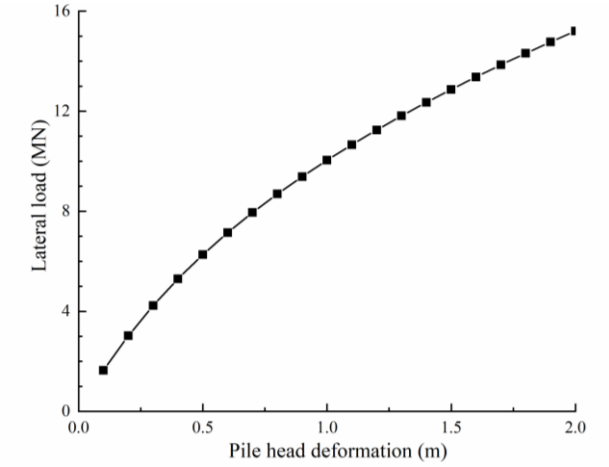

Fig. 8 Lateral load-deformation curve of the monopile

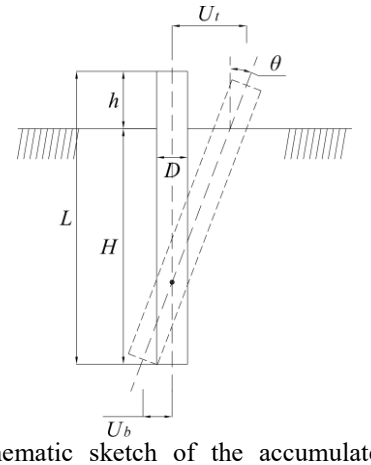

Fig. 9 Schematic sketch of the accumulated rotation angle

$$\zeta_s = \frac{M_s}{M_R}, \quad \zeta_d = \frac{M_d}{M_R} \tag{16}$$

where M_R represents the ultimate lateral load of monopile, which is determined as the pile head deformation reaches 20% of the pile diameter, as suggested by Broms *et al.* (1964). M_s and M_d stands for the one-way static lateral load and one-way cyclic lateral load, respectively.

Based on the static lateral load test results, the lateral load versus the pile head deformation is plotted in Fig. 8. According to Broms *et al.* (1964), the ultimate lateral load is determined to be M_R=13MN.

To give a clear representative of different cyclic load amplitudes on the pile performance under cyclic lateral load, the accumulated rotation angle θ is introduced and defined as

$$\theta = \sin^{-1}\left(\frac{U_t + U_b}{L}\right) \tag{17}$$

where U_t is the accumulated lateral head displacement, U_b is the accumulated lateral tip displacement and L is the length of the monopile, as illustrated in Fig. 9.

Fig. 10 indicates the accumulated rotation angle θ increases with the cyclic load ratio ζ_d under various static

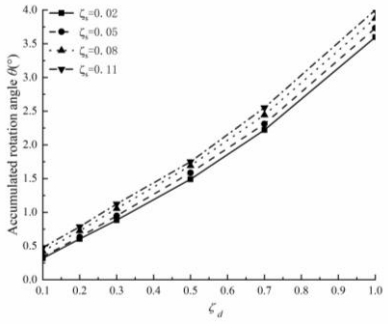

Fig. 10 Accumulated rotation angle of monopile under various ζ_s and ζ_d

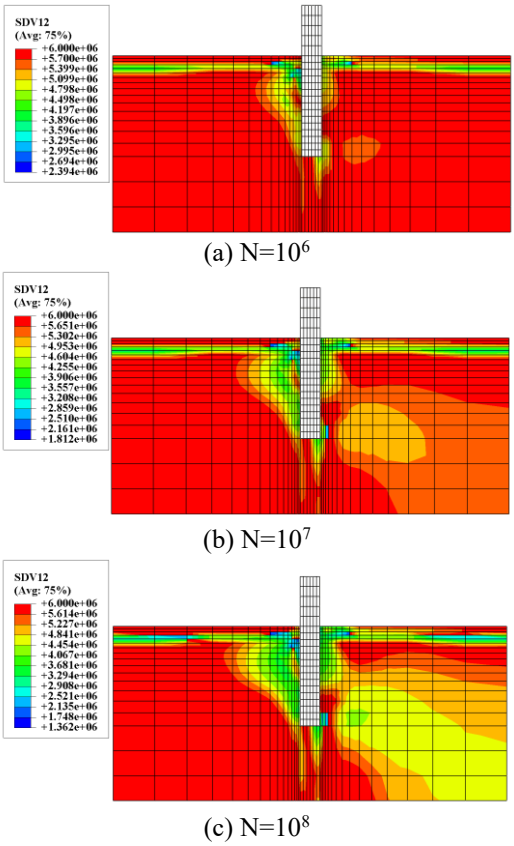

(a) N=10^6

(b) N=10^7

(c) N=10^8

Fig. 11 Stiffness degradation in pile-soil system under different load cycles

load ratios ζ_s after 10^8 load cycles. Specifically, the accumulated rotation angle θ increases linearly till the cyclic load ratio ζ_d reaches 0.5, with an increase of 22.5% as ζ_d rises from 0.1 to 0.5, whereas the accumulated rotation angle θ rises more significantly as ζ_d improves from 0.5 to 1.0. However, the rotation angle θ rises less than 5% as ζ_s increases from 0.02 to 0.11. Hence, the increase in ζ_s (i.e., static lateral load) has a marginal effect on the accumulated rotation angle θ compared with ζ_d (i.e., cyclic lateral load).

3.3 Influence of cycle number

In this study, the cyclic stiffness degradation index of soil is represented by the user-defined state variable (SDV12). Fig. 11 gives the compression modulus of soil

Table 4 The accumulated rotation angle of monopile under various L/D and L/H

Case number	Diameter D(m)	Embedded depth H(m)	L/H	L/D	Accumulated Rotation angle θ(º)
G1	6.5	40	1.5	9.2	0.605
G2	8.5	40	1.5	7.1	0.557
G3	7.5	40	1.5	8.0	0.577
G4	7.5	30	1.7	6.7	1.042
G5	7.5	50	1.4	9.3	0.386

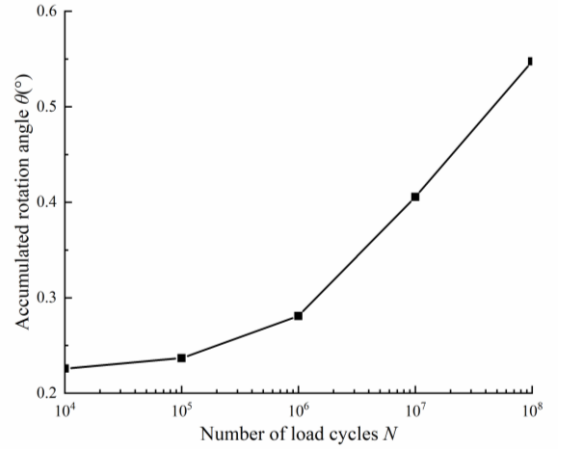

Fig. 12 The variation of aaccumulated rotation angle of monopile with the number of load cycles

element after 10^6, 10^7 and 10^8 load cycles with ζ_s=0.1 , ζ_d=0.15. It is observed that the stiffness degradation occurs in the vicinity of monopile. Specifically, the soil stiffness degradation mainly concentrated on the passive earth pressure zone, and the soil stiffness decreases with an increase of cycle number, whereas the soil stiffness degradation in the active earth pressure zone is negligible.

Fig. 12 presents the various of accumulated rotation angle of monopile with the number of load cycle. It is observed that with the cycle number rises from 10^4 to 10^6, the accumulated rotation angle θ merely increases by 9.4%, whereas the rotation angle θ increases by 139% as the cycle number reaches 10^8. Thus, the lateral deformation of monopile develops significantly as the cycle number reaches 10^6.

3.4 Influence of diameter and embedded depth

In this study, the influence of length-to-diameter ratios (L/D) and length-to-embedded depth ratios (L/H) on the accumulated rotation angle of monopile under cyclic lateral loads are investigated, with the one-way cyclic load amplitude M_d=2MN, and static lateral load is M_s=1.3MN after 10^8 cycle number. The embedded depth H and pile diameter D are related to the relative stiffness K_{rc} of monopile, which is defined as (Kishore *et al.* 2009)

$$K_{rc} = \frac{E_{pE} I_{pE}}{E_s H^4} \tag{18}$$

in which E_{pE} denotes the equivalent elastic modulus of steel pipe pile, I_{pE} is the equivalent inertial moment of steel pipe

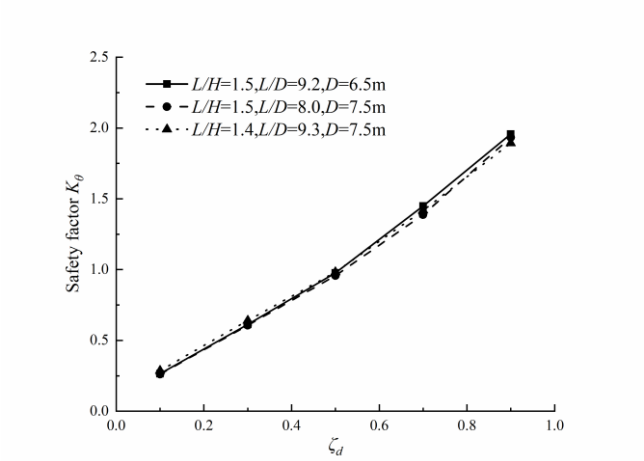

(a) Cycle number N= 10^7

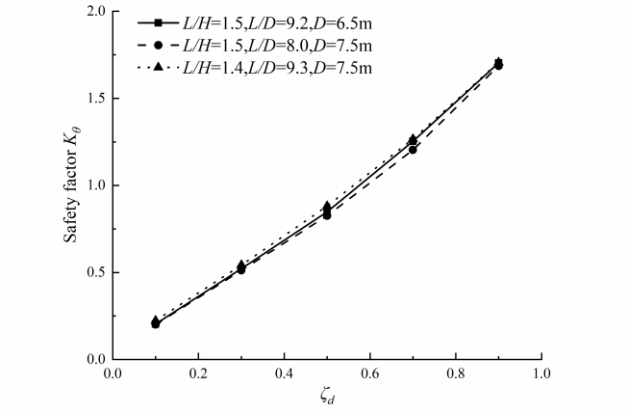

(b) Cycle number N= 10^8

Fig. 13 Variation of safety factor with cyclic load ratio under different number of cycles

pile, E_s is the compressive modulus of soil, and H is the embedded depth. When K_{rc} is larger than 0.01, the monopile is regarded as rigid. Under the given length-to-diameter ratios L/D and length-to-embedded depth ratios L/H in Table 4, the monopiles are determined to be rigid, the variation of the accumulated rotation angle of monopile for various L/D and L/H are illustrated in Table 4. As can be seen, the accumulated rotation angle of monopile increases significantly with L/H.

According to Achmus *et al*. (2009), the maximum allowed accumulated rotation angle of monopile at seabed level should be less than 0.5º to ensure the safety operation

of the offshore wind turbine. However, the accumulated rotation angle of monopile reaches 1.042º with L/H=1.7 and L/D=6.7, which is far beyond the maximum allowed accumulated rotation angle of 0.5º, and the pile foundation deforms linearly as the accumulated rotation angle of the monopile reaches 0.5°, thus the design criterion is supposed to be too conservative.

Moreover, the accumulated rotation angle reduces by 50% as L/H decreases from 1.7 to 1.5, L/D increases from 6.7 to 7.1, whereas the accumulated rotation angle decreases by 36% as L/H decreases from 1.5 to 1.4 with constant L/D=9.2. By comparison, the accumulated rotation angle θ merely decreases by 8% as L/D decreases from 9.2 to 7.1 with L/H=1.5. Therefore, it can be induced that the failure of monopile foundation can be significantly weakened by decreasing the embedded depth ratio L/H of monopile, and the applicable ranges of monopile are suggested to be L/H=1.4~1.5 and L/D=8.0~9.3, respectively.

4. Bearing capacity analysis

Tuladhar *et al.* (2008) reported that the reduction in soil stiffness leads to the reduction in the lateral bearing capacity of monopile. In this section, the variation of the accumulated rotation angle and pore pressure under cyclic lateral load are discussed by introducing the safety factor, some useful design guidelines are suggested.

4.1 Accumulated rotation angle

To give a clear representation of accumulated rotation angle on the pile performance under cyclic lateral loads, the safety factor K_θ is introduced as

$$K_\theta = \frac{\theta}{\theta_R} \tag{19}$$

where θ_R represents the rotation angle corresponding to the static ultimate lateral load capacity of the monopile.

According to the previous studies, the accumulated lateral displacement increases significantly as the cycle number reaches 10^6, and the static load ratio ζ_s has a marginal effect on the bearing capacity of monopile compared with the cyclic load ratio ζ_d.

In the following discussions, the influence of ζ_d on the bearing capacity of monopile foundation is investigated with constant ζ_s=0.1. Figs. 13(a) and 13(b) plots the variation of safety factor K_θ versus the cyclic load ratio ζ_d under different cycle numbers N=10^7, 10^8. It is observed that the safety factor K_θ shows a similar nonlinear growth trend with the cyclic load ratio under various L/H and L/D. Specifically, K_θ reaches 1.0 as ζ_d increases to 0.6 with N=10^7, and K_θ reaches 0.9 as ζ_d rises to 0.5 with N=10^8. Therefore, it is suggested that ζ_d should be less than 0.5 to ensure the safe operation of monopile foundations subjected to long-term cyclic lateral load.

4.2 Accumulated pore pressure

Under the cyclic lateral load, the pore pressure around the monopile foundation accumulates. In order to investigate the effect of pore pressure on the bearing capacity of monopile in saturated soft clay, the accumulated pore pressure safety factor K_u is defined here as

$$K_u = \frac{u}{u_0} \tag{20}$$

in which u is the accumulated pore pressure under cyclic load and u_0 is the initial static pore pressure.

Figs. 14(a)-14(f) illustrates the variation of safety factor K_u along the seabed depth with constant ζ_d=0.5, ζ_s=0.1, and N=10^7 for various distance from the central axis of monopile, i.e., x= $\pm$ 0.8D, $\pm$ 1.1D, $\pm$ 1.6D, respectively. Under one-way cyclic lateral load, K_u first increases and then decreases with the seabed depth. In the active earth pressure zone x>0, K_u is smaller than 1.15 for x is less than 1.6D, the maximum K_u occurs in the range of 0.7< z/H <0.8 for x=1.1D, whereas the maximum K_u occurs in the range of 0.5< z/H <0.6 for x increases to 1.6D. In the passive earth pressure zone x<0, K_u is smaller than 1.23 for x is less than 1.6D, the maximum K_u occurs in the range of 0.3< z/H <0.4 for x=1.1D, whereas the maximum K_u occurs in the range of 0.6< z/H <0.7 for x increases to 1.6D. In general, the pore pressure safety factor K_u is larger in the passive earth pressure zone, which indicates that the stiffness degradation of soil is more significant in the passive earth pressure zone.

For comparison, Fig. 15 plots K_u versus z/H under N=10^8, the maximum K_u are 1.23 and 1.35 in the active and passive earth pressure zone, respectively. As can be seen, the accumulated pore pressure increases slightly with cycle number

5. Conclusions

In this study, an improved stiffness degradation model considering the effect of accumulated strain and pore pressure has been proposed and implemented with the finite element method. The established stiffness degradation model is proposed for soft clay and the results of the drained cyclic triaxial tests in a numerical model can be used to estimate the progressive deformation of a monopile embedded in soft clay under long-term cyclic lateral load. Compared with the constitutive model requiring iterative calculation, the calculation efficiency of the proposed model is highly improved, which is more convenient for engineering application. Based on the numerical simulation of the pile-soil interaction system, the following conclusions are presented:

- The increase in static load ratio has a marginal effect on the accumulated rotation angle compared with the cyclic load ratio. Specifically, the accumulated rotation angle of monopile increases linearly with the cyclic load ratio as which is less than 0.5, whereas the accumulated rotation angle increases nonlinearly as the cyclic load ratio is more than 0.5, which poses a potential damage to the safety operation of monopile. Thus, the cyclic load ratio is suggested to be less than 0.5 for the monopile foundations subjected to long-term cyclic lateral load.
- The failure of the monopile foundation can be

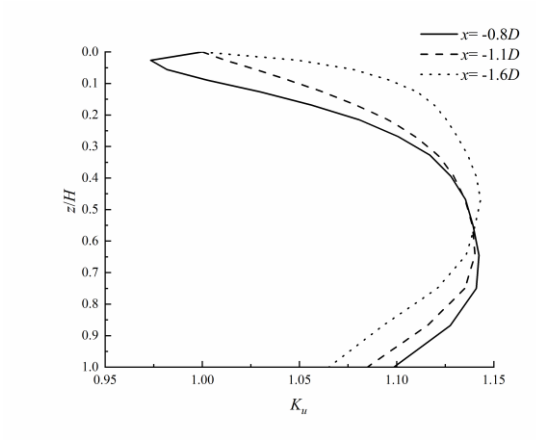

Active earth pressure zone
(a) D=7.5 m, H=40 m

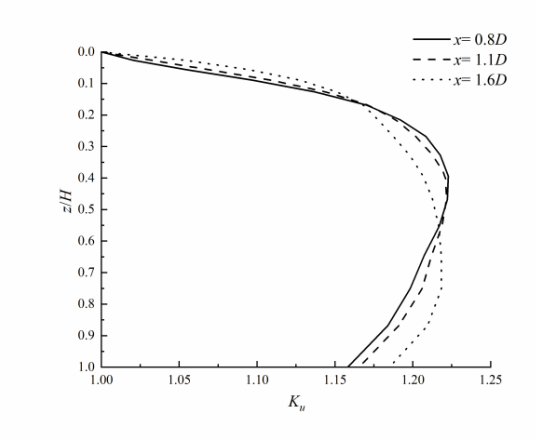

Passive earth pressure zone
(b) D=7.5 m, H=40 m

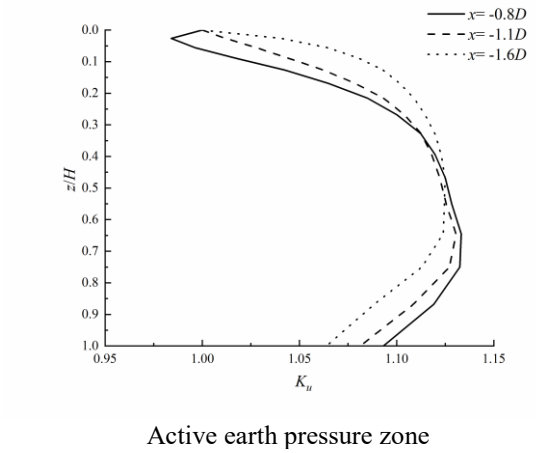

Active earth pressure zone
(c) D=6.5 m, H=40 m

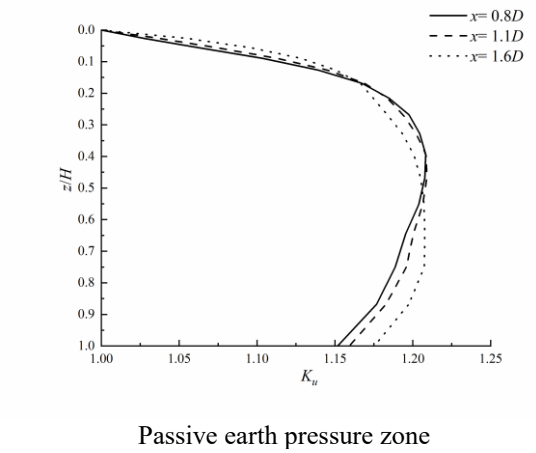

Passive earth pressure zone
(d) D=6.5 m, H=40 m

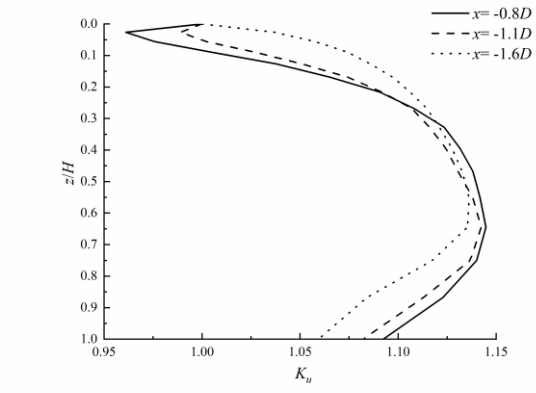

Active earth pressure zone
(e) D=7.5m, H=50 m

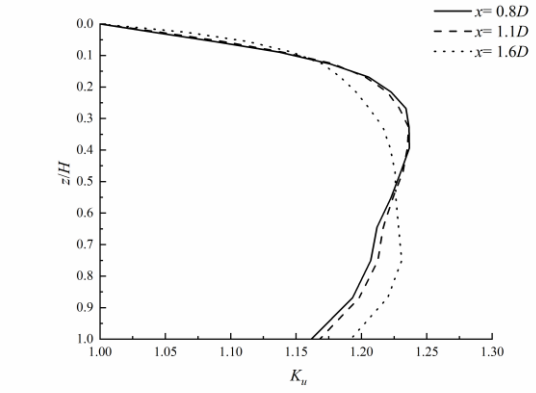

Passive earth pressure zone
(f) *D*=7.5 m, *H*=50 m

Fig. 14 The variation of safety factor with seabed depth under N=10^7

significantly weakened by decreasing the embedded depth ratio *L/H* of monopile, and the applicable ranges of monopile are suggested to be *L/H*=1.4~1.5 and *L/D*=8.0~9.3, respectively.

• The number of load cycles *N* can significantly affect the accumulated rotation angle of monopile. For the large-diameter monopile foundation, the accumulated rotation angle significantly increases with the number of load cycles *N* as *N* is larger than 10^6.

• The accumulated pore pressure distribution along the pile merely changes with pile diameter, embedded length, and the number of load cycles. The stiffness degradation of soil is more significant in the passive earth pressure zone, in which soil liquefaction is likely to occur.

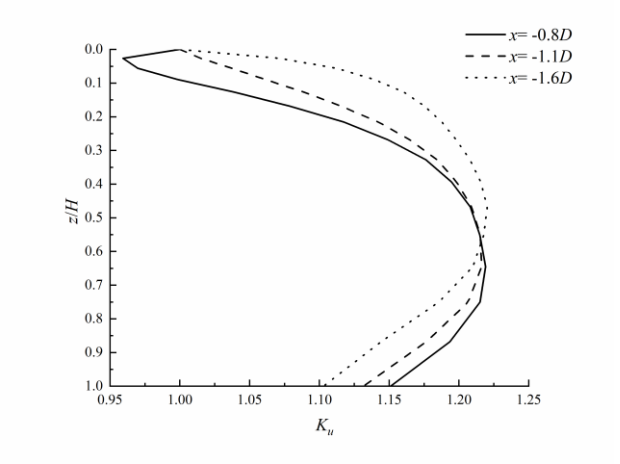

Active earth pressure zone with
(a) D=7.5 m, H=40 m

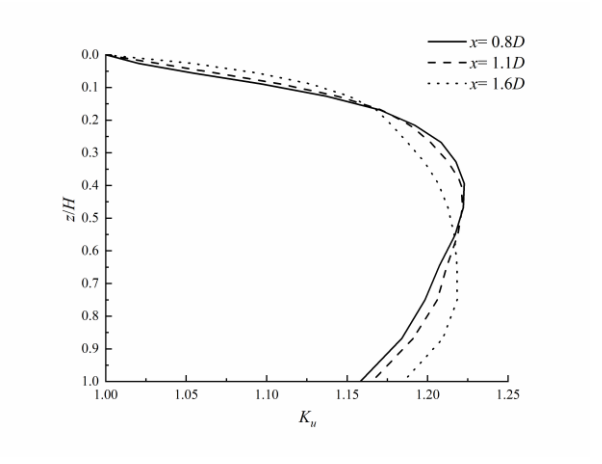

Passive earth pressure zone with
(b) D=7.5 m, H=40 m

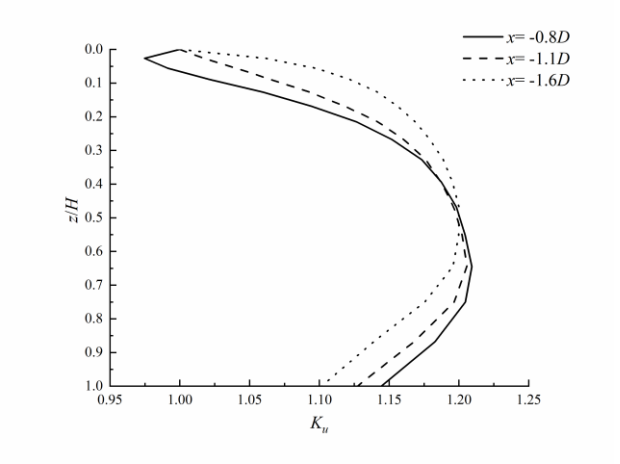

Active earth pressure zone
(c) D=6.5 m, H=40 m

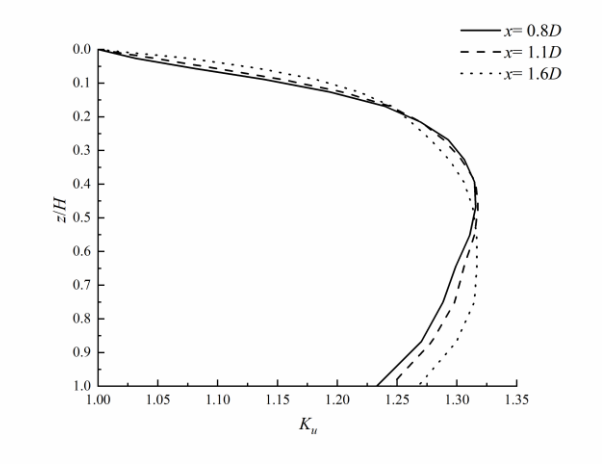

Passive earth pressure zone
(d) D=6.5 m, H=40 m

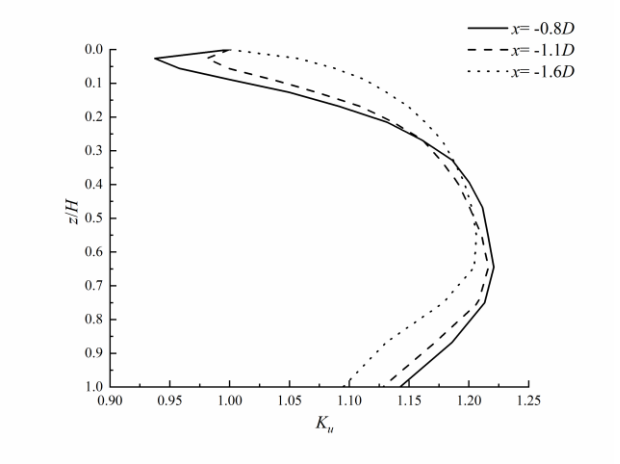

Active earth pressure zone
(e) D=7.5m, H=50 m

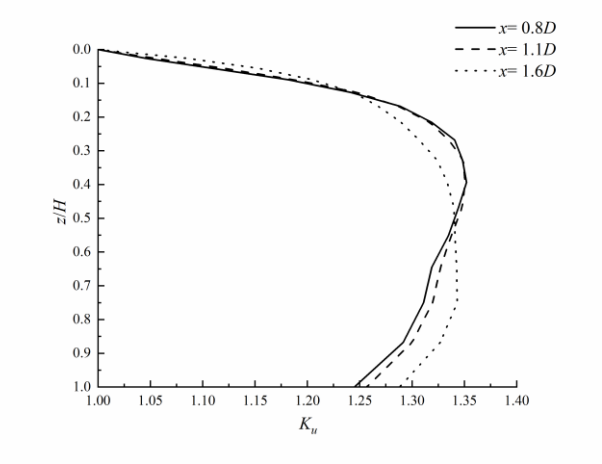

Passive earth pressure zone
(f) *D*=7.5 m, *H*=50 m

Fig. 15 The variation of safety factor with seabed depth under N=10^8

Acknowledgments

This article was funded by National Natural Science Foundation of China (No. 52178353).

References

Achmus, M., Kuo, Y.S. and Abdel-Rahman, K. (2009), "Behavior of the monopile foundations under cyclic lateral load", *Comput. Geotech.*, **36**(5), 725-735.

https://doi.org/10.1016/j.compgeo.2008.12.003.
Abhinav, K.A. and Saha, N. (2019), "Effect of stiffness degradation of clay in the dynamic response of monopile-supported offshore wind turbines", *Geotech. Appl.*, **13**, 331-339. https://doi.org/10.1007/978-981-13-0368-5_35.
Barari, A., Zeng, X.W., Rezania, M. and Ibsen, L.B. (2021), "Three-dimensional modeling of monopiles in sand subjected to lateral loading under static and cyclic conditions", *Geomech. Eng.*, **26**(2), 175-190. https://doi.org/10.12989/gae.2021.26.2.175.
Broms, B. (1964), "The lateral response of piles in cohesionless soils", *J. Soil Mech. Found. Eng. Division ASCE*, **90**(3), 123-156.
Charlton, T.S. and Rouainia, M. (2021), "Cyclic performance of a monopile in spatially variable clay using an advanced constitutive model", *Soil Dyn. Earthq. Eng.*, **140**, 106437. https://doi.org/10.1016/j.soildyn.2020.106437.
Cuéllar, P., Baeβler, M. and Rücker, W. (2013), "Relevant factors for the liquefaction susceptibility of cyclically loaded offshore monopiles in sand", *Poromechanics V: Proceedings of the Fifth Biot Conference on Poromechanics*, 1336-1345. https://doi.org/10.1061/9780784412992.160.
Cui, H.N. and Liu, X.L. (2019), "Effect of shear stiffness degradation on accumulation of pore water pressure in marine sediments", *J. Mar. Environ. Eng.*, **10**(3), 165-180.
Cui, Z.D., Zhang, L.J. and Zhan, Z.X. (2023), "Dynamic shear modulus and damping ratio of saturated soft clay under the seismic loading", *Geomech. Eng.*, **32**(4), 411-426. https://doi.org/10.12989/gae.2023.32.4.411.
Depina, I., Le, T.M.H., Eiksund, G. and Benz, T. (2015), "Behavior of cyclically loaded monopile foundations for offshore wind turbines in heterogeneous sands", *Comput. Geotech.*, **65**, 266-277. https://doi.org/10.1016/j.compgeo.2014.12.015.
Feizi, S., Arnesen, K., Aaslid, A. and Bergan-Haavik, J. (2023), "Validation of earthquake analysis methodology of a suction-caisson foundation-structure through model testing", *Mar. Struct.*, **88**, 103368. https://doi.org/10.1016/j.marstruc.2023.103368.
Gao, Z.T., Feng, X.Y., Zhang, Z.T., et al. (2022) "A brief discussion on offshore wind turbine hydrodynamics problem". *Journal of Hydrodynamics* **34**(1), 15–30. https://doi.org/10.1007/s42241-022-0002-y.
Guth, S., Katsidoniotaki, E. and Sapsis, T.P. (2023), "Statistical modeling of fully nonlinear hydrodynamic loads on offshore wind turbine monopile foundations using wave episodes and targeted CFD simulations through active sampling", *Wind Energy*, **27**(1), 75-100. https://doi.org/10.1002/we.2880.
Gerolymos, N. and Gazetas, G. (2005), "Constitutive model for 1-D cyclic soil behaviour applied to seismic analysis of layered deposits", *Soils Found.*, **45**(3), 147-159. https://doi.org/10.3208/sandf.45.3_147.
Gotschol, A. (2009), "Veränderlich elastisches und plastisches Verhalten nichtbin-diger Böden und Schotter unter zyklisch-dynamischer Beanspru-chung", Herausgegeben im Eigenverlag, Kassel, Hessian, Germany.
Hu, A.F., Zhang, G.J. and Jia, Y.S. (2014), "Application of degradation stiffness model in analysis of cumulative lateral displacement of monopile foundation", *J. Zhejiang Univ. (Engineering Science)*, **48**(4), 721-726. https://doi.org/10.3785/j.issn.1008-973X.2014.04.023.
Huang, M.S., Li, J.J. and Li, X.Z. (2006), "Cumulative deformation behaviour of soft clay in cyclic undrained tests", *Chinese J. Geotech. Eng.*, **28**(7), 891-895.
Huurman, M. (1996), "Development of traffic induced permanent strain in concrete block pavements", *Heron*, **41**(1), 29-52.
Idriss, I.M., Dobry, R. and Singh, R.D. (1978), "Nonlinear behavior of soft clays during cyclic loading", *J. Geotech. Eng. Division*, **104**(12), 1427-1447. https://doi.org/10.1061/AJGEB6.0000727.
Kishore, Y.N., Rao, S.N. and Mani, J.S. (2009), "The behaviour of laterally loaded piles subjected to scour in marine environment", *KSCE J. Civil Eng.*, **13**(6), 403-408.
Kuo, Y.S., Achmus, M. and Abdel-Rahman, K. (2012), "Minimum embedded length of cyclic horizontally loaded monopiles", *J. Geotech. Geoenviron. Eng.*, **138**(3), 357-363. https://doi.org/10.1061/(ASCE)GT.1943-5606.0000602.
Lei, J., Wang, Y., Zhang, B, Li, F. and Liu, C. (2022), "Cyclic and post-cyclic characteristics of marine silty clay under the multistage cycling-reconsolidation conditions", *Ocean Eng.*, **258**. https://doi.org/10.1016/j.oceaneng.2022.111803.
Liu, J.M., Fu, H.Q. and Guo, T.T. (2020), "Comparative experimental study on dynamic characteristics of soft clay under different cyclic loads", *China Earthq. Eng. J.*, **42**(4), 973-981. https://doi.org/10.3969/j.issn.1000-0844.2020.06.973.
Matasović, N. and Vucetic, M. (1995), "Generalized cyclic-degradation-pore-pressure generation model for clays", *J. Geotech. Eng.*, **121**(1), 33-42. https://doi.org/10.1061/(ASCE)0733-9410(1995)121:1(33).
Shi, Y.X., Cheng, Y.Z. and Huang, X.Y. (2022), "Numerical simulation of unsteady flow field around monopile under the combined influence of wave and vibration", *Ocean Eng.*, **276**, 114238. https://doi.org/10.1016/j.oceaneng.2023.114238.
Thiers G.R., Seed H.B. (1968), "Cyclic stress-strain characteristics of clay", *J. Soil Mech. Found. Division*, **94**(2), 555-569. https://doi.org/10.1061/JSFEAQ.0001110.
Tuladhar, R., Maki, T. and Mutsuyoshi, H. (2008), "Cyclic behavior of laterally loaded concrete piles embedded into cohesive soil", *Earthq. Eng. Struct. D.*, **37**(1), 43-59. https://doi.org/10.1002/eqe.744.
Werkmeister, S. (2003), "Permanent deformation behaviour of unbound granular materials in pavement constructions", Technischen Universität Dresden, Dresden, Germany.
Wang, Y., Lei, J., Gong, X., Wang, Y. and Yang, P. (2018), "Post-cyclic undrained shear behavior of marine silty clay under various loading conditions", *Ocean Eng.*, **158**:152-161. https://doi.org/10.1016/j.oceaneng.2018.03.081.
Wang, Y., Qi, Z., Wei, T., Bao, J., Zhang, X. and Zhou, Y. (2023), "Numerical study on the responses of suction pile foundations under horizontal cyclic loading considering the soil stiffness degradation", *J. Mar. Sci. Eng.*, **11**(12), 2336. https://doi.org/10.3390/jmse11122336.
Yasuhara, K., Yamanouchi, T. and Hirao, K. (1982), "Cyclic strength and deformation of normally consolidated clay", *Soils Found.*, **22**(3), 77-91. https://doi.org/10.3208/sandf1972.22.3_77.
Yu, D.W., Ye, J.H. and Yun, C.Q. (2023), "Dynamics of offshore wind turbine and its seabed foundation under combined wind-wave loading", *Ocean Eng.*, **286**, 115624. https://doi.org/10.1016/j.oceaneng.2023.115624.
Zhao, C.Y, Zhou, S.H. and Li, Z. (2012), "Cyclic accumulative pore pressure model of soft clay in the Shanghai region", *J. China Railway Soc.*, **1**,77-82. https://doi.org/10.3969/j.issn.1001-8360.2012.01.014.

GC